

# Coupled Electromagnetic and Thermal Analysis of Single-Phase Insulated High-Current Busducts and GIL Systems

Petar Sarajcev<sup>1,\*</sup>, Ivo Martinac<sup>2</sup>, Zdenko Radic<sup>2</sup>

<sup>1</sup>Department of Electrical Power Systems, University of Split, FESB, Split, Croatia

<sup>2</sup>Project biro Split, Ltd, Split, Croatia

\*Corresponding author: petar.sarajcev@fesb.hr

Received March 27, 2013; Revised April 15, 2013; Accepted April 19, 2013

**Abstract** This paper presents a mathematical model for the coupled electromagnetic and thermal analysis of the single-phase insulated high-current busducts of circular cross-section geometry and of gas-insulated transmission lines (GIL). The mathematical model, accompanied by a numerical solution procedure, features an exact current distribution in phase conductors and shields of the busduct or GIL system, accounting for the skin and proximity effects, and including the complete electromagnetic coupling between phase conductors and shields. The current distribution is based on the conductor filament method in combination with the mesh-current method. The mathematical model further couples the analysis of current distribution with the computation of (Joule) power losses and subsequent temperature increase in the high-current busducts or GIL systems, accounting for the material properties (electrical conductivity, thermal emission and convection coefficients) as well as for the surrounding ambient properties (ambient temperature, wind and solar radiation influences).

**Keywords:** high-current busduct, gas-insulated transmission line (GIL), electromagnetic and thermal analysis, filament method, mesh-current method, geometric mean distance

## 1. Introduction

High-current busduct systems are air-insulated, often also single-phase-insulated, enclosure transmission lines with tubular (or sometimes hexagonal) aluminum conductors encapsulated in the coaxial aluminum enclosure (i.e., shield). They facilitate very efficient way of evacuating power from the generator units, especially in case of, e.g., hydro power plants [1,2,3].

Gas-insulated transmission lines (GIL) represent high-voltage electric power transmission technology suitable for very efficient transmission of bulk electric power across both short and long distances [4,5,6]. The insulating media is often N<sub>2</sub>-SF<sub>6</sub> gas mixture; pure SF<sub>6</sub> is rarely used, except on very short distances. The insulating media, thus, facilitates the geometry of the GIL system being very similar (in terms of the cross-section geometry) to that of the high-current busducts. Hence, mathematical models of the high-current busducts are directly applicable to the analysis of GIL systems, allowing for the small differences in design and manufacturing details. The GIL technology is increasingly becoming very popular in bulk transmission of electric power across long distances, e.g., [4,7-11]; it could be laid on the earth's surface, buried in the earth or installed in tunnels, e.g., in existing railway tunnels, e.g., [4,8]. The GIL technology has several promising features, such as: low transmission losses, low capacitive load, power rating of the equivalent overhead

transmission line, high reliability, no electric ageing, no thermal ageing, operation equal to that of the overhead transmission line (i.e., auto-reclosure of the relay protection functions), low environmental influence, etc.

The shields of the high-current busducts could be grounded on a single end or on both ends (with additional possibility for grounding at several places along the route). With GIL systems, shields are continuously grounded along the transmission line route, e.g., [4,6]. Additionally, shields of different phases are mutually bonded (i.e., short-circuited with appropriate current-carrying conductors) along the route, both for the high-current busducts and GIL systems. This establishes the current paths for the so-called circulating currents (along with eddy currents) in the shields, which oppose the phase currents (inducing them) through the strong electromagnetic coupling (additionally influenced by the skin and proximity effects), e.g., [12,13,14].

Both phase conductor current and (induced) shield current distribution generate (Joule) power losses, which in-turn produce heating of the phase conductors and shields. The power losses depend on the conductor material properties (electrical conductivity, thermal emission and convection coefficients), while the temperature increase (in the phase conductors and shields) not only depend on the material properties but are additionally influenced by the ambient (i.e., environmental) conditions (e.g., ambient temperature, wind and solar radiation influences).

This paper presents a mathematical model for the coupled electromagnetic and thermal analysis of single-phase insulated high-current busducts (of circular cross-section geometry) and of GIL systems. The mathematical model, accompanied by a numerical solution procedure, features an exact current distribution in phase conductors and shields of the busduct or GIL system, accounting for the skin and proximity effects, and including the complete electromagnetic coupling between phase conductors and shields. The current distribution is based on the subdivision of the phase conductors and shields into the conductor filaments and the subsequent application of the mesh-current method, with the aid of the geometric mean distance method (GMD). The mathematical model further couples the analysis of current distribution with the computation of (Joule) power losses and temperature increase in the high-current busducts or GIL systems, accounting for the material properties of the busduct (or GIL), as well as the surrounding ambient properties. Various shield grounding and bonding treatments could be accounted for, as well as different operating conditions of the busduct or GIL system at hand.

The approach presented in this paper differs in terms of the problem domain decomposition from the finite element method (FEM) approach, which has been seen as a standard method of approach in dealing with this category of problems, and has been implemented in several commercially available software packages, e.g., [15]. Here presented method of approach is more efficient than the FEM procedure (in general terms), in treating the busduct and/or GIL system, due to the fact that the FEM approach – in this open boundary problem – needs to carry-out discretization of the very large solution region, e.g., [15]. On the other hand, filament method only needs the discretization of the busduct system itself (i.e., its cross-sectional geometry), thus resulting in a far lower number of (finite) elements (i.e., filaments). Furthermore, this method of approach is far easier to implement – in terms of the computer codes – than FEM approach, for solving the coupled electromagnetic and thermal problems of high-current busduct and/or GIL systems.

## 2. Mathematical Model

The mathematical model for the coupled electromagnetic and thermal analysis of high-current busduct (or GIL) features an iterative solution procedure. Analysis starts by dividing the busduct (or GIL) cross-section geometry into the large number of conductor filaments and deriving their position within the (arbitrarily positioned) global coordinate system.

At this point the iteration loop begins. A system of complex linear algebraic equations is formed, based on the self and mutual impedances between the conductor filaments, while accounting for the initial and terminal conditions. Solution of this system of equations yields the current distribution in the cross-section geometry of the busduct (or GIL) system, where the skin and proximity effects have been inherently absorbed. Next, based on the initial, i.e., ambient temperature conditions, the (Joule) power losses in the busduct (or GIL) system are computed (from the filament currents), accounting for the

temperature-dependent electrical conductivity of the material.

Using the computed power losses, the temperature increase of the phase conductors and shields are determined, taking into account the thermal emission and convection coefficients of the material (e.g., painted conductor surfaces, etc.), and possibly the wind and solar radiation influences. The temperature increase influences the electrical conductivity of the material, thus in-turn, influencing the power losses. From these newly-obtained temperatures of the phase conductors and shields, new values of the electrical conductivity of the material are determined (for the phase conductor and shield) and another iteration step is carried-out, computing new current distribution and associated power losses, from which the temperature increase is again determined. This process is repeated until the steady state is reached, determined by the final, i.e., steady-state temperatures for the assumed operating and ambient conditions (i.e., when there is no additional change in the computed temperatures between successive iterations, accounting for the selected tolerance margin of course).

### 2.1. Conductor Filaments

Each phase conductor of the high-current busduct (or GIL) system is divided into  $N_c$  filaments (i.e., subconductors), while each shield is divided into  $N_s$  filaments; coordinates of the filaments are determined in regards to the global coordinate system (positioned arbitrarily). Hence, the total number of filaments equals  $N = 3N_c + 3N_s$ . Mentioned numbers of filaments for the phase conductors and shields are chosen in such a manner that the current density remains uniform across the surface (of each) of the filaments [12].

Subsequently, the Carson's theory is employed for determining the self and mutual impedances of the loops, which involves the computation of the associated distances between the filaments as a prerequisite step. Here a geometric mean distance (GMD) method is employed for that purpose, accounting for the fact that the filaments are rectangular in cross-section. Figure 1 depicts a part of the geometry involved in deriving the self and the mutual GMD of phase conductor and/or shield filaments.

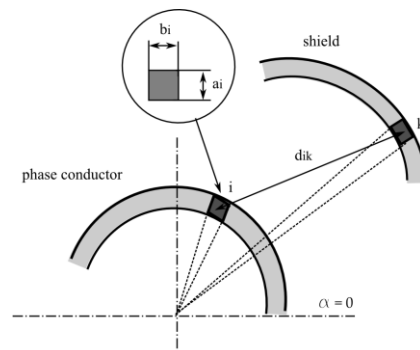


**Figure 1.** Depiction of the geometry involved in determining the self and mutual GMD of filaments

For the arbitrary  $i$ -th filament of a rectangular cross section, the self GMD is given by [12]:

$$d_{ii} = 0.2235 \cdot (a_i + b_i) \quad (1)$$



power losses. In the process of determining these currents skin and proximity effects have been accounted for, as well as the material conductivity (which is temperature dependent). Knowing the filament currents, the losses of the phase conductors carrying phases L1, L2, L3 are respectively computed from the following relations [12,21,22]:

$${}^{ph}P_{L1} = \sum_{i=1}^{Nc} |\bar{I}_i|^2 \cdot R_i(T) \quad (8)$$

$${}^{ph}P_{L2} = \sum_{i=Nc+1}^{2Nc} |\bar{I}_i|^2 \cdot R_i(T) \quad (9)$$

$${}^{ph}P_{L3} = \sum_{i=2Nc+1}^{3Nc} |\bar{I}_i|^2 \cdot R_i(T) \quad (10)$$

while that of the appropriate shields are given by [12,21,22]:

$${}^{sh}P_{L1} = \sum_{i=3Nc+1}^{3Nc+Ns} |\bar{I}_i|^2 \cdot R_i(T) \quad (11)$$

$${}^{sh}P_{L2} = \sum_{i=3Nc+Ns+1}^{3Nc+2Ns} |\bar{I}_i|^2 \cdot R_i(T) \quad (12)$$

$${}^{sh}P_{L2} = \sum_{i=3Nc+2Ns+1}^{3Nc+3Ns} |\bar{I}_i|^2 \cdot R_i(T) \quad (13)$$

The temperature dependent  $i$ -th filament resistance  $R_i(T)$  in the above expressions, regardless of the conductor type (phase conductor or metal shield), is computed according to the following expression:

$$R_i(T) = \frac{\ell}{\kappa(T) \cdot S_i} \quad (14)$$

where:  $\kappa(T)$  - temperature-dependent conductivity of the (non-magnetic) material of the phase conductor or shield, at the appropriate temperature (T); phase conductor and shield will have different operating temperatures (although they might be of the same material),  $S_i$  - surface of the cross sectional area of the filament,  $\ell$  - filament length (i.e., busduct or GIL length).

From the above obtained power losses, the temperature increase of the busduct (or GIL) phase conductors and shields are determined for each of the phases as follows (equations are here provided for the phase L1 only), [24,25,26]:

$${}^{ph}P_{L1} = 5.67\pi \cdot d_1 \cdot \frac{\left(\frac{T_{ph} + 273}{100}\right)^4 - \left(\frac{T_{sh} + 273}{100}\right)^4}{\frac{1}{\varepsilon_1} + \frac{d_1}{d_2} \cdot \left(\frac{1}{\varepsilon_2} - 1\right)} + \frac{K_1 \cdot (P+1)^n \cdot d_1^{0.75} \cdot (T_{ph} - T_{sh})^{1.25}}{\left[\ln\left(\frac{d_2}{d_1}\right) + 2.2\right] \cdot \left[1 + \left(\frac{d_1}{d_2}\right)^{0.6}\right]^{1.25}} \quad (15)$$

$${}^{ph}P_{L1} + {}^{sh}P_{L1} + \varepsilon_3 d_3 \cdot P_{sol} = 5.67\pi \cdot \varepsilon_3 \cdot d_3 \cdot \left[ \left(\frac{T_{sh} + 273}{100}\right)^4 - \left(\frac{T_{amb} + 273}{100}\right)^4 \right] + K_2 \cdot d_3^{0.75} \cdot (T_{sh} - T_{amb})^{1.25} + K_3 \cdot (v \cdot d_3)^m \cdot (T_{sh} - T_{amb}) \quad (16)$$

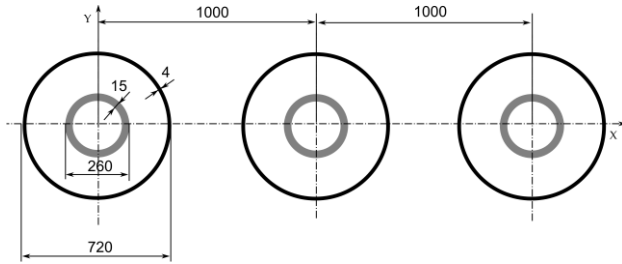
where:  $d_1$  - outer diameter of the phase conductor (m);  $d_2$ ,  $d_3$  - inner and outer diameters of the shield (m);  $\varepsilon_1$  - emissivity coefficient of the phase conductor outer surface (untreated surface: 0.1, treated with black Almite: 0.9);  $\varepsilon_2$  - emissivity coefficient of the shields inner surface (untreated: 0.1, painted black: 0.9);  $\varepsilon_3$  - emissivity coefficient of the shields outer surface (untreated: 0.1, painted with Munsell N7: 0.8)  $K_1$  - convection constant between phase conductor and shield, which depends on the insulation media (80%–20%  $N_2$ - $SF_6$  gas mixture: 16.8, pure  $SF_6$  gas: 4.4);  $K_2$  - convection constant between the shield and the ambient air (2.75) =  $K_3$  - convection constant representing effect of wind (7.5);  $P$  - insulating gas pressure (kgf/cm<sup>2</sup> at 20 °C);  $n$  - exponent of the  $SF_6$  gas pressure (0.65)  $m$  - exponent corresponding to the Reynolds number (0.6);  $T_{ph}$  - temperature of the phase conductor (°C);  $T_{sh}$  - shield temperature (°C);  $T_{amb}$  - ambient temperature (°C);  $P_{sol}$  - solar radiation (W/m<sup>2</sup>);  $v$  - wind velocity (m/s). For more information about the derivation process of the non-linear equations (15) and (16), with particular emphasis on the wind influence, consult [25].

These equations were in-fact derived by the application of the well-known Stefan-Boltzman formula for the radiative heat transfer, where various constants have been experimentally obtained, see [25] for additional information and necessary explanations. The system of the two obtained non-linear equations, given by (15) and (16) for the phase L1, are numerically solved for the temperatures of the phase conductors and shields; along with the associated non-linear equations for the other two phases (giving 3x2=6 non-linear equations in total). This is here carried-out by the modified Powell hybrid algorithm and a finite-difference approximation to the associated Jacobian matrix, which has been implemented in the developed computer program by the appropriate subroutines of the IMSL library [27].

Once the temperatures become known a new iteration step commences. Starting from the new values of the material conductivity (at this new phase conductors and shields temperatures), new resistance values are computed from (14) for each and every filament associated with all phase conductors and shields. With that, the system of equations in (4) is constructed again and numerically solved for the filament currents. Then, a new set of Joule power losses are determined from equations (8) to (13), accounting for the changed filament electrical conductivity. This in-turn provides the new input values for the set of two non-linear equations (15) and (16) per phase, which are again numerically solved for the yet-new temperatures. This iterative process continues until the steady-state is reached (computed temperatures between successive iterations remain the same, accounting for the selected tolerance margin of course).

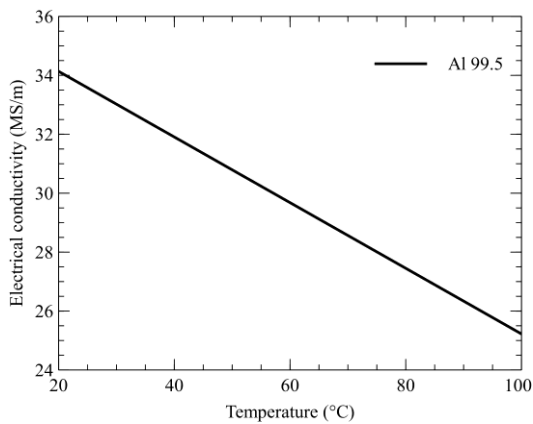
### 3. Numerical Example

Figure 2 graphically depicts the cross-section of the high-current and air-insulated generator busduct under consideration. Dimensions are given in millimeters. Rated voltage of the busduct system at hand is assumed to be 24kV (phase-to-phase) with designed rated continuous operating current of 7000A. Length of the busduct system is assumed to be 100meters. For the relative soil resistivity of the site a value of 100Ωm is provided.



**Figure 2.** Dimensions of the high-current generator busduct under consideration

Phase conductors and shields are assumed to be made of high-quality aluminum (Al 99.5) with conductivity of 34.2MS/m at 20 °C, e.g., [3]. Maximum allowable operating over-temperature of the phase conductors must not exceed 65 °C above the temperature of the surrounding medium (i.e., air). Also, maximum allowable over-temperature of the shield must not exceed 40 °C above the temperature of the surrounding medium. The temperature of the surrounding medium (air) is taken equal to 40 °C. Figure 3 graphically depicts the functional relationship between the temperature of the Al 99.5 material and its electrical conductivity, which is used in the solution procedure.



**Figure 3.** Temperature-dependent electrical conductivity of the Al 99.5 busduct material

According to the procedure for the numerical solution of the filament current distribution, each phase conductor of the busducts (viewed in cross-section) is subdivided into 500 filaments (three concentric layers of equal thickness; first two layers having 150 filaments each, while the third one having 200 filaments). Additionally, each shield of the high-current busduct is subdivided into 400 filaments, giving a total of 2700 filaments. It is assumed that the shields of the generator busduct system are grounded on both ends and that they are furthermore mutually bonded (i.e., short-circuited) on both ends (of the

route). This gives rise to the circulating currents in the shields (along with eddy currents), as well as the earth-return current between the grounding systems at both ends of the busduct route. Furthermore, it is assumed that the phase conductors outer surface is painted black. Also, the inner surface of the shield is painted black as well, while its outer surface is painted with Munsell N7 (i.e., gray color). The influence of the surface treatment (i.e., painting black) on the temperature increase will be examined later in the paper. Additionally, the influence of the wind and solar radiation / insolation on the changes of the busduct steady-state temperature will be examined later in the paper as well.

Table 1 presents results of the numerical computation, carried-out by the computer program developed by the authors (based on the presented mathematical model), of the current distribution in the phase conductors and shields of the high-current busduct at hand. It can be nicely observed from this table that the shield currents are almost equal to the phase currents (even larger in one of the phases), due to the fact that there are current paths, formed by the shield bonding, giving rise to the so-called circulating currents.

**Table 1** Current distribution in the high-current generator busduct

Currents	I (A) ∠ (°)		
	Phase L1	Phase L2	Phase L3
Phase conductors	6997 ∠ -0.3 °	6997 ∠ 239.7 °	6997 ∠ 119.7 °
Shields	6847 ∠ 182.8 °	6977 ∠ 64.7 °	7122 ∠ -57.1 °
Earth	12.1 ∠ -24 °		

It is quite evident from the data presented in this table that the shield currents do not form a symmetric three-phase system; there is an asymmetry present among the shield currents, which is due to the inherent electromagnetic asymmetry found in the flat formation of the three-phase conductor arrangements, e.g. [21,22].

Table 2 presents numerically computed Joule power losses of the high-current busduct, relevant for the proposed operating condition (i.e., rated current of 7000 A) and shield treatment, accounting for the reached operating steady-state temperatures of the phase conductors and shields.

**Table 2** Power losses in the high-current generator busduct

Power losses	P (W/m)		
	Phase L1	Phase L2	Phase L3
Phase conductors	173	173	173
Shields	177	184	192
Total	1072		

According to the analysis carried out by the commercially available software package MagNet, [15], the total power losses of 1088W/m have been obtained for the busduct at hand. Comparison of this result with that from the table II yields a relative difference of 1.47 %, which is mainly due to the differences in treating, i.e., imposing the busduct operating conditions (as well as some minor differences in the busduct geometry), [28]. This could be seen as a very good agreement between two

different numerical approaches in the treatment of the same problem. Furthermore, the laboratory tests of this configuration (carried-out by Končar Steel Structures Inc.) confirm the numerically obtained current distribution and power losses.

Additionally, Figure 4 presents a power loss distribution (in the filaments) in the shields of the busduct system, where the leftmost phase conductor carries phase L1, middle one carries phase L2 while the rightmost one carries the phase L3. Position of the filaments in each of the shields is given in its local cylindrical coordinate system, whose origin coincides with the center of the each phase, while the angle displacement commences at the positive x-axis of the global coordinate system and increases in the counter-clockwise direction (observe Figure 1 Figure 2). It can be easily deduced from the Figure 4 that the power loss distribution in the shields is not centrally-symmetrical, due to the influence of the proximity effects on the current distribution in the shields.

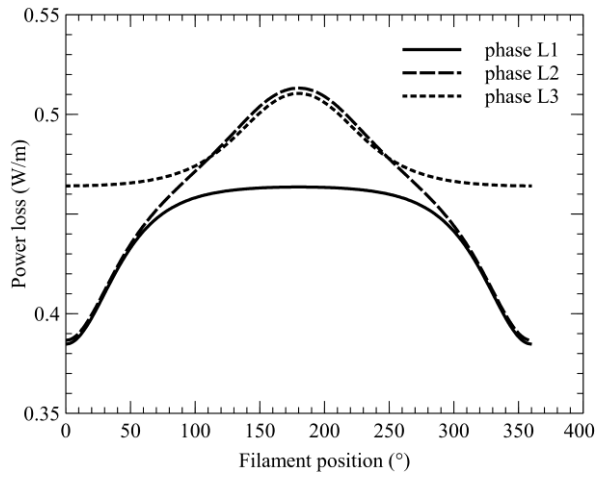


Figure 4. Power loss distribution in the shields of the busduct system

Furthermore, Table 3 presents the steady-state temperatures of the phase conductors and shields of the busduct at hand, computed for the above mentioned operating condition (using the ambient temperature of 40 °C) and shield grounding and bonding treatment as has been previously described.

Table 3. Temperatures of the high-current generator busduct

Currents	T ( °C )		
	Phase L1	Phase L2	Phase L3
Phase conductors	76.3	76.6	77
Shields	59	59.3	59.7

According to the numerical solution carried out with the commercial software package MagNet, [15], the steady-state temperature of the phase conductor equals 77 °C, while that of the shield equals 59 °C, [28]. By comparing these values with those from the Table 3 it becomes quite evident that the obtained results are in an excellent agreement. This analysis has been in-fact carried-out without the influence of the wind or solar insolation. These same findings have been confirmed by the laboratory tests, carried-out by Končar Steel Structures Inc. It is evident that the maximum allowable temperature of the phase conductor (105 °C) has not been reached; neither has been reached the maximum allowed temperature of the shield (80 °C).

Hereafter, we present the analysis of the wind and solar radiation influences on the busduct temperature. Firstly, the steady-state temperatures of the busduct at hand are determined as a function of the current that the busduct is carrying. This will define the so-called default condition. Regarding this condition, we will further analyze the influence of the not-painting the conductor and shield surfaces, as well as the wind and solar radiation influences on the obtained steady-state temperatures (as just mentioned). The shield grounding and bonding conditions will not be changed in the subsequent analysis. The ambient temperature is fixed at 40 °C for all further analysis.

Figure 5 graphically presents the functional relation between the obtained steady-state temperatures of the busduct phase conductor and shield (average values between three phases) and the symmetrical three-phase currents that flow through the busduct system. This figure represents the mentioned default condition.

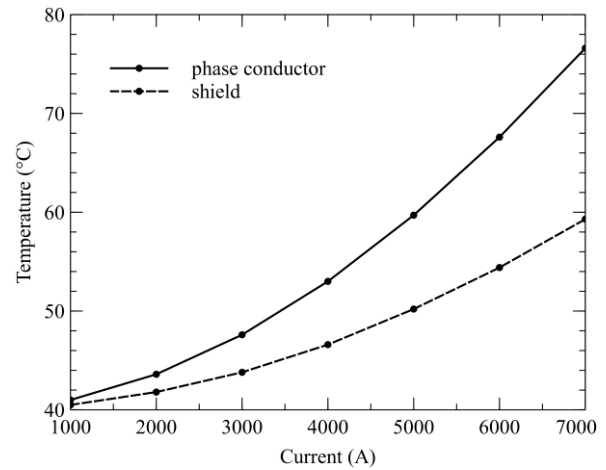


Figure 5. Steady-state temperatures of the phase conductor and shield as a function of the current carried by the busduct (default condition)

In order to assess the influence of the painting black the outer surface of the phase conductor and the inner surface of the shield, let us now assume that these surfaces are not treated (i.e., not painted). Figure 6 depicts the steady-state temperatures obtained for this case of untreated surfaces, as a function of the busduct current. For the reference, the default case is provided in the same figure as well.

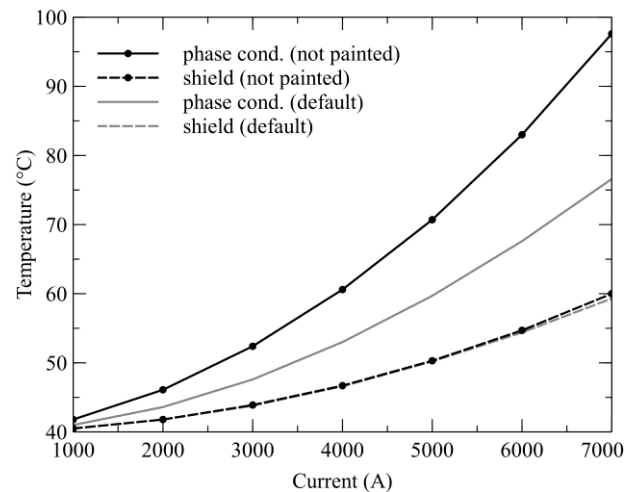


Figure 6. Steady-state temperatures of the phase conductor and shield for different surface treatments (i.e., painting black or not)

It can be nicely observed from this figure that the painting of the conductors black significantly reduces the steady-state (operating) temperature of the phase conductors, which could be seen as beneficial. Moreover, the obtained steady-state temperature of the phase conductor in this case, for the rated (nominal) operating current of 7000A, critically approaches the maximum allowed temperature for the phase conductor, which is here given as 105 °C (ambient temperature of 40 °C).

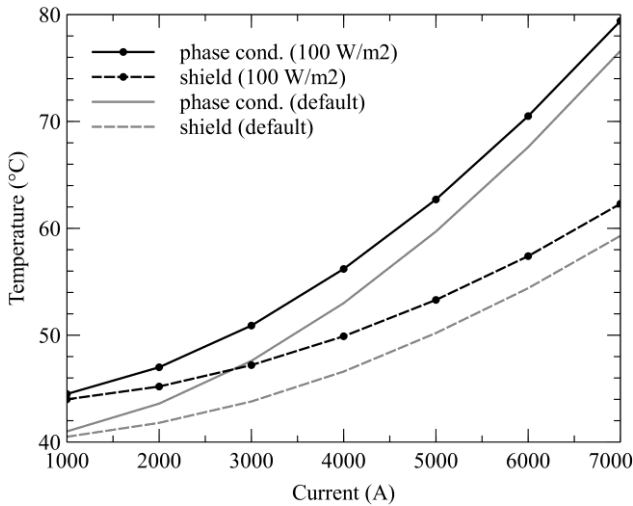


Figure 7. Steady-state temperatures of the phase conductor and shield under the solar insolation of 100 W/m<sup>2</sup>

Furthermore, let us examine the influence of the solar radiation, i.e., solar insolation on the steady-state temperature increase of the busduct phase conductors and shields. The surface of the phase conductor and shields are treated as explained at the beginning of this section (i.e., inner surface painted black with the gray outer surface). Figure 7 depicts the steady-state temperatures of the phase conductor and shield for the busduct exposed to the solar insolation of 100W/m<sup>2</sup>. The default case is provided in this figure, for the reference, as well. It is quite evident from the Figure 7 that the solar radiation increases the steady-state temperature of the phase conductor and shield. This is important to account for where the busduct is constructed in the open air and exposed to the solar radiation influence.

It could be stated here that without painting the surface of the phase conductor (and the inner surface of the shield) in black paint, the solar influence would most-probably drive the steady-state temperature of the phase conductor, for the rated current of 7000A, above the maximum allowed temperature. This is certainly not to be tolerated.

Finally, let us examine the influence of the wind conditions on the obtained steady-state temperatures of the busduct at hand. The surface of the phase conductor and shields are again assumed to be treated as explained at the beginning of this section (i.e., painted black). In that regard, Figure 8 provides the computed steady-state temperatures of the busduct (as a function of busduct current) obtained under the influence of the wind with the velocity of 1 m/s. It is quite evident from the Figure 8 that the presence of the wind decreases the obtained steady-state temperatures of the busduct (both for the phase conductors and shields), thus, having the opposite effect from that of the solar radiation. This could be seen as beneficial.

It should be noted that it has been assumed throughout this analysis (presented in Figure 5, Figure 6, Figure 7 and Figure 8) that the outer surface of the shields has been painted in gray color (Munsell N7).

In the end, Figure 9 presents the results of the analysis of the influence of different wind velocities on the temperature drop obtained for the phase conductor and shield steady-state temperatures (compared with the default case). It can be observed from this figure that the 1 m/s wind decreases the phase conductor steady-state temperature for 4.5 °C and that of the shield for 4.7 °C. It is also evident that the reduction of the shield temperature is somewhat larger than that of the phase conductor. Thus, it could be stated that the wind influence somewhat reduces compensates the influence of the solar radiation (if present).

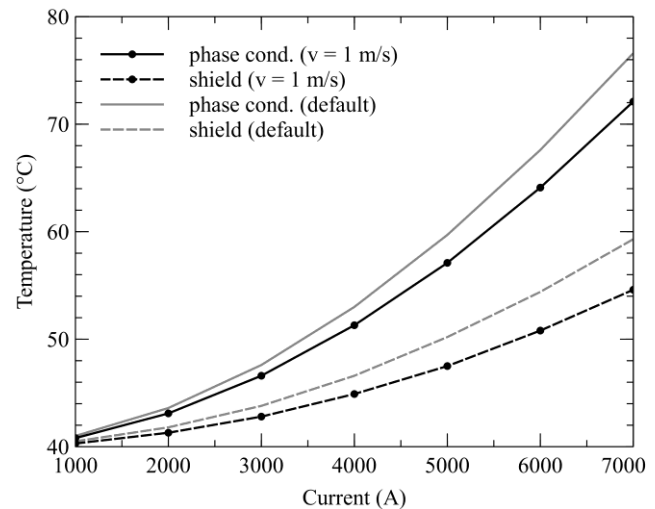


Figure 8. Steady-state temperatures of the phase conductor and shield under the influence of 1 m/s wind

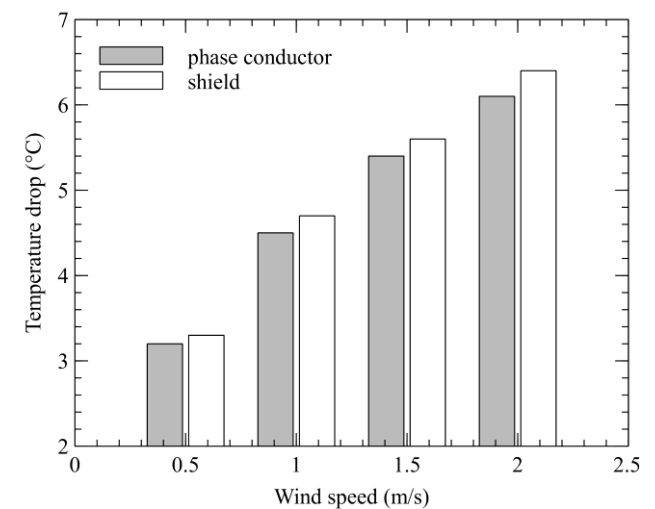


Figure 9. Phase conductor and shield steady-state temperature drop under the influence of wind

The analysis provided here (carried-out with the computer program developed on the basis of the presented mathematical model) could be further expanded to incorporate the combined influences of the wind and the solar radiation, for different operating conditions (both for the balanced and unbalanced load currents, as well as for the various short-circuit conditions). Hence, this methodology could be applied in the design process of the

high-current busduct (or GIL), for example, in order to determine the cross-section area for the needed nominal (operating) current, while at the same time satisfying the needed maximum over-temperatures of the phase conductors and shields. This could be seen valuable, considering that the application (particularly) of the high-voltage GIL systems is expected to increase in the near future, e.g., in offshore wind farm applications and for bringing the bulk transmission power to major city centers, [29,30].

## 4. Conclusion

This paper presented a computational (numerical) model for the coupled electromagnetic and thermal analysis of the current distribution, Joule power losses and steady-state temperatures in the high-current busducts and GIL systems. The presented methodology incorporates the skin and the proximity effects in the electromagnetic coupling between phase conductors and shields of the busduct or GIL systems, accounting as well for the exact cross-section geometry and temperature-dependent material properties. Mathematical model for the current distribution itself is based on the application of the filament method, combined with the mesh-current method and the geometric mean distance method. Different operating conditions, along with different shield grounding and bonding treatments could be accounted for by this approach.

The coupled electromagnetic and thermal model features an iterative solution procedure, where the temperatures of the phase conductors and shields, obtained from the power loss computation (itself influenced by the exact current distribution and material properties), become input data for the next iteration step of the solution procedure, hence, reaching the steady-state only after several iteration steps. Temperature-dependent conductivity of the busduct or GIL material features prominently in this analysis.

Furthermore, influence of the solar radiation and wind velocity is also incorporated in the mathematical (computational) model. Hence, studies of these influences are combined with the analysis of the current distribution and power losses in the phase conductors and shields; they are inter-dependent. Also, treatment of the surfaces of the phase conductors and shields and their repercussions on the steady-state temperature increase (further exacerbated by the solar and wind influences) is also studied.

The analysis provided in this paper has been corroborated by the comparison of the computational results obtained by the computer program developed on the basis of the theory presented here and those obtained from the commercially available software package. Very good agreement between results has been found, both for the power losses and the steady-state temperatures. On top of that, the developed computer program is numerically very efficient and rather easy to develop.

In the end, it could be stated that the methodology provided in this paper could be effectively applied during different stages of the design process for the single-phase-insulated high-current busducts of circular cross-section geometry, as well as for the GIL systems of different high-

voltage levels, while accounting for the installation provisions at the same time.

## References

- [1] ABB, *Generator Busduct, Power Technology Systems*, ABB AG, Mannheim, Germany, 2009. [Online] Available: <http://www.abb.com> [Accessed: Jan. 10, 2013].
- [2] GE Energy, *Segregated and Non-Segregated Bus Ducts*, GE, St-Augustine, Quebec, Canada. [Online] Available: [http://www.genenergy.com/prod\\_serv/products/bus\\_ducts/en/seg\\_and\\_non\\_seg.htm](http://www.genenergy.com/prod_serv/products/bus_ducts/en/seg_and_non_seg.htm) [Accessed: Jan. 10, 2013].
- [3] Končar, *Isolated Phase Busbar Solutions*, Končar—Metal Constructions, Zagreb, Croatia. [Online]. Available: [http://www.koncar-k.hr/kmk\\_isolated\\_phase\\_busbars\\_3\[en\].htm](http://www.koncar-k.hr/kmk_isolated_phase_busbars_3[en].htm) [Accessed: Jan. 10, 2013].
- [4] Siemens, *Gas-Insulated Transmission Lines (GIL)*, Siemens AG, Erlangen, Germany, 2010.
- [5] Kunze, D., Binder, E., Türk, J., Pöhler, S., Alter, J., "Gas-Insulated Transmission Lines—Underground Power Transmission Achieving a Maximum of Operational Safety and Reliability," in *Proceedings of the International Conference on Insulated Power Cables (JICABLE '07)*, Paris-Versailles, France, 24-28 June 2007.
- [6] Koch, J. "Experience with 2nd Generation Gas-Insulated Transmission Lines GIL," in *Proceedings of the International Conference on Insulated Power Cables (JICABLE '03)*, Paris-Versailles, France, 22–26 June 2003, Paper A.3.2.
- [7] Drews, A., et. al., Network of offshore wind farms connected by gas insulated transmission lines, [Online]. Available: [www.forwind.de/forwind/files/ewec2008\\_gil3-1.pdf](http://www.forwind.de/forwind/files/ewec2008_gil3-1.pdf) [Accessed: Jan. 10, 2013].
- [8] Benato, R., "Gas Insulated Transmission Lines in Railway Galleries," *IEEE Transactions on Power Delivery*, 20, 704-709. 2005.
- [9] Menke, P., *Innovative Solutions for Bulk Power Transmission*, Siemens AG, Erlangen, Germany, 2011.
- [10] Koch, H., Schuette, A., "Gas insulated transmission lines for high power transmission over long distances," *Electric Power Systems Research*, 44, 69-74. 1998.
- [11] Alberta Energy, *Assessment and Analysis of the State-of-the-Art Electric Transmission Systems with Specific Focus on High-Voltage Direct Current (HVDC), Underground or Other New or Developing Technologies*, Alberta Energy, Stantec, Canada, 2009.
- [12] Sarajčev, P., Goić, R., "Power loss computation in high-current generator bus ducts of rectangular cross-section," *Electric Power Components and Systems*, 38, 1469-1485. 2010.
- [13] Piatek, Z., "Total Eddy Currents Induced in Screens of a Symmetrical Three-Phase Single-Pole Gas-Insulated Transmission Line (GIL)". [Online] Available: <http://advances.utc.sk/index.php/AEEE/article/download/94/147> [Accessed: Jan. 10, 2013].
- [14] Benato, R., Dughiero, F., Forzan, M., Paolucci, A., "Proximity effect and magnetic field calculation in GIL and in isolated phase bus ducts," *IEEE Transactions on Magnetics*, 38, 781-784. 2002.
- [15] Infolytica, *MagNet v7: 2D/3D Electromagnetic Field Simulation Software* [Online] Available: <http://www.infolytica.com/en/products/magnet/> [Accessed: Jan. 10, 2013].
- [16] Kovač, N., Sarajčev, I., Poljak, D., "Nonlinear-coupled electric-thermal modeling of underground cable systems," *IEEE Transactions on Power Delivery*, 21, 4-14. 2006.
- [17] Kovač, N., Sarajčev, I., Poljak, D., "Nonuniformity modeling of a particular aluminum sheath temperatures and losses," *IEE Proceedings of Generation, Transmission and Distribution*, 153, 553-559. 2006.
- [18] Sarajčev, P., "Numerical Analysis of the Magnetic Field of High-Current Busducts and GIL Systems," *Energies*, 4, 2196-2211. 2011.
- [19] Carson, J.R., "Wave propagation in overhead wires with ground return," *Bell Systems Technical Journal*, 5, 539-554. 1926.
- [20] Dommel, H.W., *EMTP Theory Book*, Microtran Power System Analysis Corporation, Vancouver, Canada, 1992.
- [21] Sarajčev, I., *Power loss computation of cable systems*, Ph.D. Dissertation, University of Zagreb, FER, Zagreb, Croatia, 1985 (in Croatian).

- [22] Sarajčev, I., Majstrovic, M., Medić, I., "Calculation of Losses in Electric Power Cables as the Base for Cable Temperature Analysis," in B. Sunden & C. A. Brebbia (Eds.), *Advanced Computational Methods in Heat Transfer VI*, WIT Press, Southampton, 2000, pp. 529-537.
- [23] Lapack, *Linear Algebra Package, Ver. 3.2.1, User's Guide*, 3rd Edition, Society for Industrial and Applied Mathematics, 1999.
- [24] Benato, R., Dughiero, F., "Solution of Coupled Electromagnetic and Thermal Problems in Gas-Insulated Transmission Lines," *IEEE Transactions on Magnetics*, 39(3). 1741-1744. 2003.
- [25] Minaguchi, D., Ginno, M., Itaka, K., Furukawa, H., Ninomiya, K., Hayashi, T., "Heat Transfer Characteristics of Gas-Insulated Transmission Lines," *IEEE Transactions on Power Delivery*, 1(1). 2-9. 1986.
- [26] Itaka, K., Akari, T., Hara, T., "Heat Transfer characteristics of Gas Spacer Cables," *IEEE Transactions on Power Apparatus and Systems*, 97. 1579-1585. 1978.
- [27] Visual Numerics, *IMSL: Fortran Subroutines for Mathematical Applications*, Math/Library Volumes 1 and 2, Visual Numerics, 1997.
- [28] Končar, *Technical Solution of the High-Current Generator Busducts Design for the HPP Zakučac along with Electrical Equipment Selection*, Končar, Zagreb, 2007. (in Croatian).
- [29] Koch, H., Benato, R., Laußegger, M., Kähler, M., Leung, K.K., Mirebeau, P., Kindersberger, J., Kunze, D., di Mario, C, Renaud, F., Bowmann, G., "Application of long high capacity gas-insulated lines in structures," *IEEE Transactions on Power Delivery*, 22. 619-626. 2007.
- [30] Awad, R., Peacock, C., Benato, R., Butt, I., de Wild, F., Takahashi, Y., Jeyapalan, J.K. Kim, J.T., Monteys, J., Moreau, C., Oberger, K., Sakuma, S., Woschitz, R., Yoon, K.T., "Cable Systems in Multi Purpose or Shared Structures," CIGRÉ Technical Brochure N°403, Working Group B1.08, CIGRÉ: Paris, France, February 2010.
- [31] Koch, H., et.al., "Application of long high capacity Gas-Insulated Lines in structures," CIGRÉ Technical Brochure N°351, Working Group B3/B1.09, CIGRÉ: Paris, France, October 2008.